Title
Propeller arc: design and basic characteristics

Journal
Plasma Sources Science and Technology, 27(12)

ISSN
0963-0252

Authors
Pei, Xuekai
Gidon, Dogan
Graves, David B

Publication Date
2018

DOI
10.1088/1361-6595/aaf7ef

Peer reviewed

PAPER

Propeller arc: design and basic characteristics

IOP Publishing Plasma Sources Science and Technology
Plasma Sources Sci. Technol. **27** (2018) 125007 (10pp) https://doi.org/10.1088/1361-6595/aaf7ef

Propeller arc: design and basic characteristics

Xuekai Pei, Dogan Gidon and David B Graves

Department of Chemical & Biomolecular Engineering, University of California at Berkeley, Berkeley, CA 94720, United States of America

E-mail: graves@berkeley.edu

Received 8 September 2018, revised 12 November 2018
Accepted for publication 11 December 2018
Published 28 December 2018

Abstract

A new atmospheric pressure non-equilibrium plasma source named the 'Propeller Arc' (PA) is developed using the concept of rotating electrodes. The PA device consists of a rotating cathode, driven by a motor, with one or more fixed anodes. Plasma is ignited at or near the narrowest gap as the rotating cathode passes by the anode and then it is extended up to a length of ~66 mm or longer depending on the supplied power. This allows for efficient ignition, followed by a quick increase in plasma volume. The PA is similar to the widely used gliding arc (GA); however, unlike the GA, PA does not require imposed gas flow, and the PA discharge frequency can be easily controlled by the motor angular velocity. In this paper, the basic characteristics of PA are investigated using two different operation modes: pulse modulation and DC power. Discharge properties including electrical characteristics, time-resolved optical emission images, plasma electrical properties such as resistance and average electric field (discharge voltage divided by gap distance) and plasma power consumption are reported. Use of multiple anodes to increase the plasma volume is also demonstrated. As the PA has a compact design and is relatively easy to stabilize and control without the need for applied gas flow, it has potential to be adapted for many different applications such as nitrogen fixation, fuel and carbon dioxide conversion, waste, odor and hydrogen sulfide treatment, etc.

Keywords: non-equilibrium plasma source, gliding arc, propeller arc, rotating electrodes discharge

1. Introduction

Applications of atmospheric pressure non-equilibrium plasma generally utilize energetic electrons and ions to facilitate chemical processes at a low or relatively low neutral gas temperature [1, 2]. Examples include applications in medicine [3, 4], disinfection [5], water treatment [6], material treatment [7, 8], nitrogen fixation [9, 10], food processing and agriculture [11], among many others. Many different atmospheric pressure non-equilibrium plasma generation methods have been reported to address the multiple and sometimes unique requirements of these applications [2, 12, 13].

One widely used plasma source is the gliding arc (GA) discharge [14–16]. This plasma device has been successfully used in a variety of technological applications [17–27]. The traditional 'flat' GA discharge looks similar to the 'Jacobs ladder' configuration. These devices are commonly driven by a high voltage applied across adjacent, vertically aligned and diverging electrodes. Gas breakdown to form the plasma column usually occurs at the closest gap between the two diverging electrodes. After breakdown, the discharge 'glides' up the electrodes due to natural convection from the locally heated neutral gas. In other configurations, the electrodes may not be vertically aligned and the discharge moves along the diverging electrodes through the applications of an external gas flow. The diverging geometry of the electrodes causes the length of the plasma to increase, requiring a larger voltage to sustain the plasma. At some point, the power supply is not able to deliver enough input energy to maintain the increasingly longer discharge. As a result, the discharge intensity decreases and the discharge is finally extinguished. Soon after the extinction of the GA, the discharge is re-ignited at the shortest gap again and the same elongation and extinction process re-occurs. This process repeats in a cyclic manner at relatively high frequencies depending on the speed of gas

flow and other mechanical and electrical parameters of the configuration.

GA has proven useful for many applications by reason of its simple structure, chemical selectivity, relatively high-power densities, etc. Perhaps most importantly, the moving GA discharge can treat relatively large volumes of gas at a relatively low applied voltages compared to the common pin-to-plane or pin-to-pin discharge structures. However, there are also some drawbacks to the traditional GA discharge configuration [18, 19]. Sometimes the GA configuration can be difficult to control due to instabilities and the inherently transient character of the discharge. Numerous authors have addressed the issues of GA slip velocities, plasma column lengths, and related issues [28–32]. Another aspect that can complicate use of this configuration is the need for a relatively strong gas flow which can tend to intensify the natural instabilities of GA by turbulence. Furthermore, non-uniform gas flows and relatively low gas residence time in the plasma region can limit some applications.

In response to these perceived limitations, some authors have suggested structural improvements on the original GA design. For example, Kalra *et al* [33, 34] designed a gliding arc 'tornado' (GAT), sometimes referred to as a 'plasmatron' [21, 35, 36]. These configurations exploit a reverse vortex flow in a cylindrical volume to form a three-dimensional plasma column. A GAT-like design ensures more uniform gas treatment and has a larger gas residence time in the plasma region. Gangoli *et al* [18, 19] reported a magnetically stabilized gliding arc discharge which utilizes a magnetic field to stabilize a GA plasma discharge. In this alternative, the plasma is driven as a single unit in the direction governed by the Lorentz force and moves continuously without further elongation or extinction, while electrical parameters can be controlled. Other researchers [37, 38] combined these designs and proposed a so-called 'rotating gliding arc', co-driven by a magnetic field and tangential flow. Czernichowski *et al* [39] developed the so-called 'GlidArc-II reactor', based on a rotating plate-shaped electrode driven by high-voltage AC. For this kind of discharge, forced flow of the gas is not necessary. However, documentation of basic characteristics (electrical, optical characteristics etc) of this kind of rotating electrode discharge has been limited until now.

In this paper, we will report on an alternative elongating non-equilibrium plasma source that we refer to as the 'Propeller Arc' (PA) discharge. Briefly, PA consists of a rotating cathode (ground electrode), driven by a motor, with a fixed anode (HV electrode). It is similar in some ways to a traditional GA [14, 16, 39] which also ignites at a narrow gap but, in PA the plasma region is extended by the motion of the rotating cathode rather than via an applied gas flow. One key difference between the 'GlidArc-II reactor' of Czernichowski *et al* [39], and PA is that PA can be operated using pulse modulation or via a DC power supply. The plasma column length and the discharge frequency can be adjusted and controlled accurately without applied gas flow. The discharge can be expanded to larger volume by using additional electrodes. Some basic characteristics of PA are investigated in this paper including electrical characteristics; time-resolved optical emission imaging; plasma electrical properties such as resistance and average electric field (discharge voltage divided by gap distance) and plasma power consumption. We also report some results using multiple electrodes. As the PA has a compact design and is relatively easy to stabilize and control without the need for applied gas flow it be adapted for many different applications. Some promising use cases include nitrogen fixation, fuel conversion, carbon dioxide conversion, waste and odor treatment, and hydrogen sulfide treatment, etc. It may also be relevant to studies combining plasma with heterogeneous catalysis.

2. Design and operation of the PA

Figure 1 shows one configuration of PA using pulse power modulation. The propeller-like blades of the rotating (grounded) cathode are made by stainless-steel. The distance between the center of motor axis and the tip of the cathode is 35 mm. A stainless-steel pin with a diameter of 0.8 mm is used as the stationary anode electrode. Using pulse modulation, the plasma is ignited at the narrowest gap (∼0.5 mm) between cathode and anode, and is then drawn away by the rotating electrode to a length up to ∼55 mm. Two vertical distribution of hall sensors (A3144E) were used to capture the position of the rotating cathode (see figure 1(a)). This information triggers the HV amplifier connected to the anode, controlling the ignition and extinguishment of the discharge based on the propeller location. With this design, the amplifier can apply HV to the anode when the cathode tip is at the narrowest gap. The discharge frequency is controlled by the motor angular velocity. In the results reported here, frequency can be adjusted from ∼1 Hz to 200 Hz. A ballast resistor of 0.2 MΩ is used to limit the current to less than 45 mA which is the highest current allowed for stable operation of the amplifier used (TREK MODEL 10/40 A). In this way, a relatively large plasma volume can be produced while achieving breakdown at a relatively low voltage. Figure 1(b) is a photograph of the PA discharge at 9 kV applied voltage and 60 Hz (corresponding to motor speed of 1800 revolutions per minute, rpm).

If a DC power supply (Spellman High Voltage, SL10PN1200) is used to drive the PA discharge, the configuration of the setup is simpler, as shown in figure 2. There is no need for hall sensors, signal generator or amplifier. In this case, the plasma is ignited automatically at a gap of ∼6 mm before the cathode reaches the narrowest gap, where the breakdown voltage is 9 kV. After breakdown, the development of the plasma is similar to the case with pulse modulation. The key difference is that the plasma extinguishment is not controlled and occurs naturally when the cathode is sufficiently far from the anode and the power supply is unable to deliver enough energy to maintain a plasma at the increasingly longer discharge.

In this paper, two HV voltage probes (Tektronix P6015A) were used to measure the applied voltage (V_a) and discharge gap voltage (V_{dis}) as shown in figures 1(a) and 2(a). A current probe (Pearson 6585) with a useable rise time of

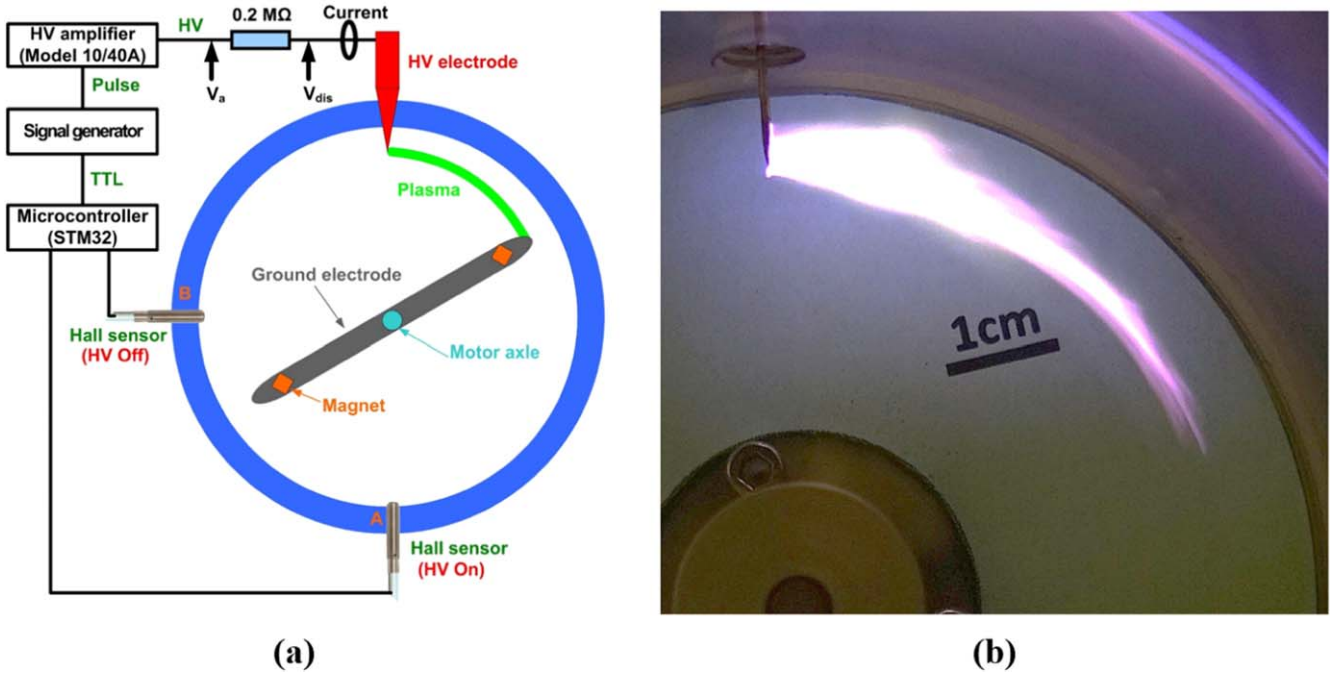

Figure 1. (a) Configuration of the PA discharge using pulse modulation. Note the electrode is moving clockwise; (b) discharge photograph with an applied voltage of 9 kV and frequency of 60 Hz.

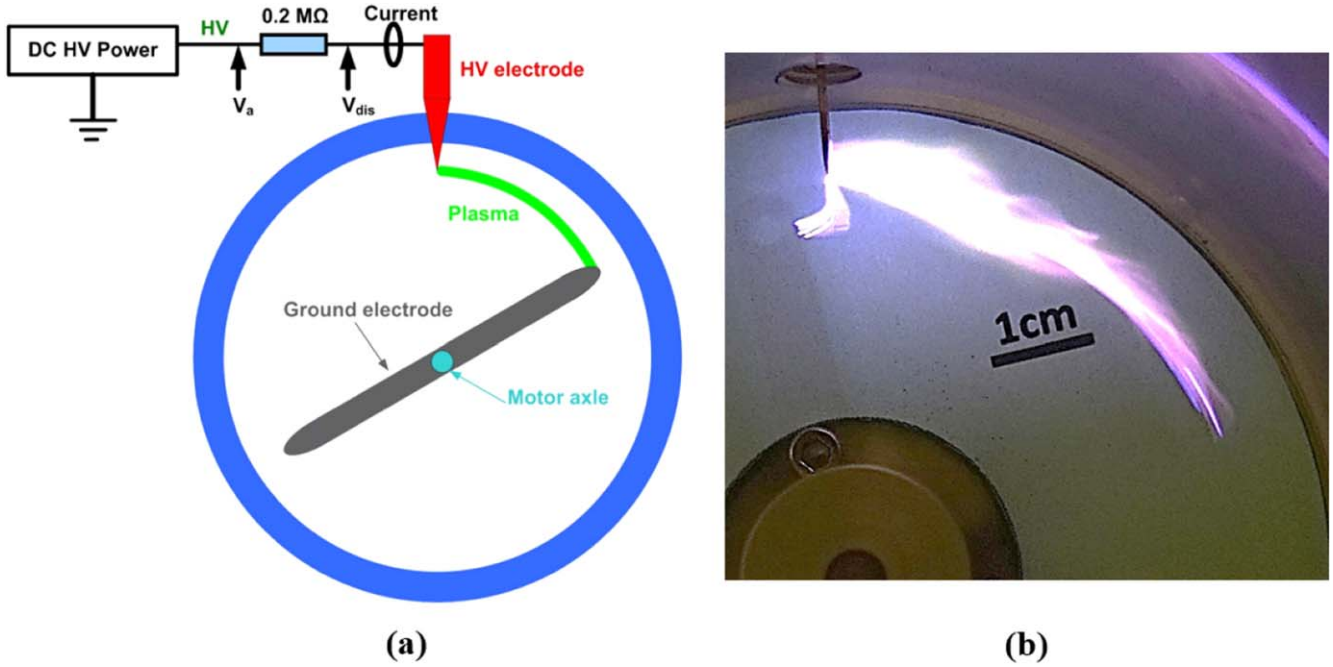

Figure 2. (a) Configuration of the PA discharge using a DC power supply; (b) corresponding discharge photograph with an applied voltage of 9 kV and frequency of 60 Hz.

1.5 nanoseconds is used to measure the breakdown region discharge current (I_{dis}). After breakdown, the current is captured by the voltage difference across the ballast resistor. The HV and current probes are linked to a 200 MHz digital oscilloscope (Tektronix TDS2024) with a sampling rate up to 2 GHz. The power consumption of PA discharge is calculated by

$$P_{dis} = f \times \int_0^t V(t) \times I(t)\mathrm{d}t. \quad (1)$$

Here, f is the discharge frequency, $V(t)$ is the gap voltage, $I(t)$ is the discharge current.

The light emitted by the PA plasma discharge is collected via optical fiber. The optical emission spectra (OES) were

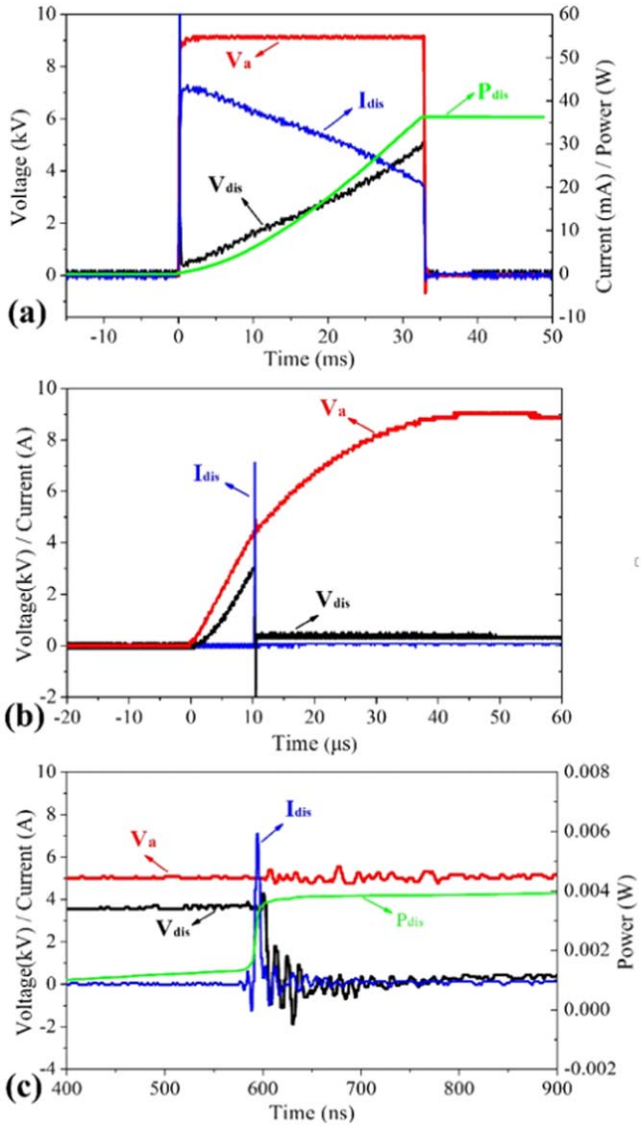

Figure 3. Waveforms of PA discharge voltage and current using pulse modulation in the time scale of ms (a), μs (b) and ns (c) with an applied voltage of 9 kV and frequency of 15 Hz. The calculated power during the pulse is illustrated in (a) for the whole discharge ($\sim$33 μs) and (c) for the breakdown region ($\sim$500 ns).

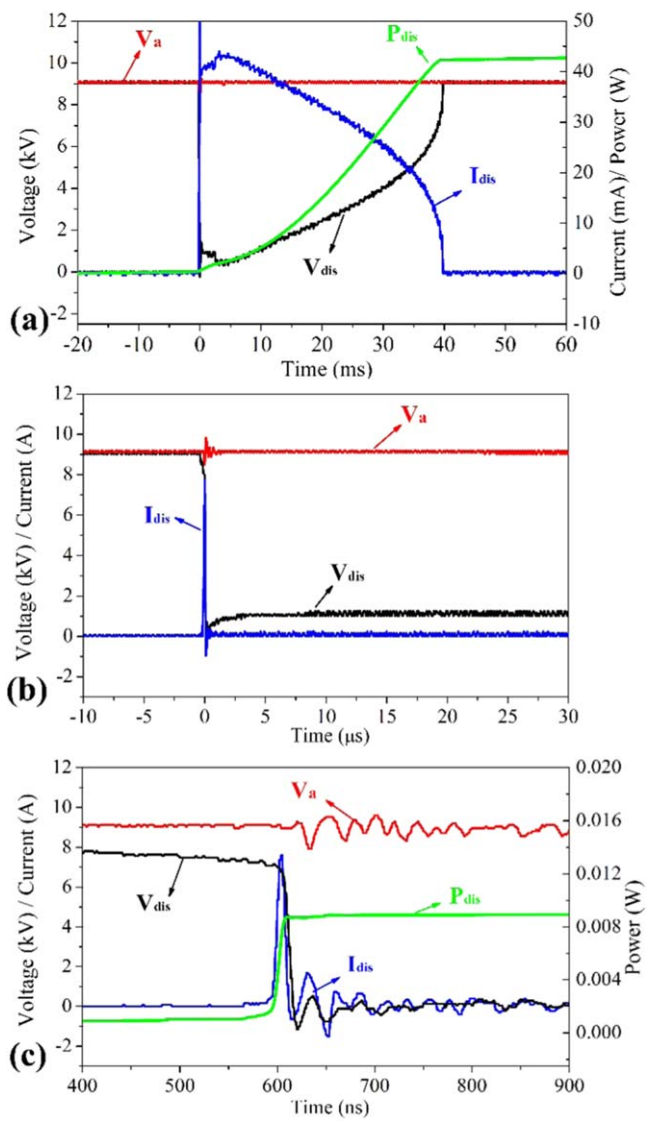

Figure 4. Waveforms of PA discharge voltage and current using a DC power supply, shown on time scales of ms (a), μs (b) and ns (c) with an applied voltage of 9 kV and frequency of 15 Hz. The calculated power during the pulse is illustrated in (a) for the whole discharge ($\sim$40 μs) and (c) for the breakdown region ($\sim$500 ns).

recorded with a USB2000 (Ocean Optics). The integration time is 200 ms and the resolution is $\sim$0.35 nm/pixel.

3. Results and discussions

3.1. Electrical characteristics of PA

Figure 3 shows the waveforms of PA discharge voltage and current using pulse modulation with three increasingly high time resolutions around the breakdown region. Breakdown occurs when the gap voltage reaches $\sim$3 kV, then discharge voltage (V_{dis}) drops to nearly zero. As the plasma plume extends in length, the V_{dis} increases to about 5 kV before the applied voltage V_a is set to zero (controlled by hall sensor B). At the same time, discharge current (I_{dis}) appears with a $\sim$20 ns pulse with a peak of $\sim$7 A during breakdown. The current peak drops to $\sim$45 mA within $\sim$0.1 μs. The discharge current decreases to $\sim$20 mA just before V_a is zeroed. The PA plasma total power consumption reaches $\sim$36 W which is significantly higher than dissipated power recorded with a pin-to-plane(2 mm gap) discharge under the same experiment conditions ($\sim$11 W). As the discharge is ignited at the point in time when the gap is narrowest (0.5 mm) and the discharge frequency (15 Hz) is low, the power consumption in the breakdown region is only $\sim$5 mW (figure 3(c)). This value is negligible compared with the overall plasma power consumption ($\sim$36 W).

From the electrical characteristics of PA illustrated in figure 3, we can see that at breakdown, the discharge appears similar to the 'transient spark' discharge reported by Janda *et al* [40]. The transient spark is a filamentary, streamer-to-

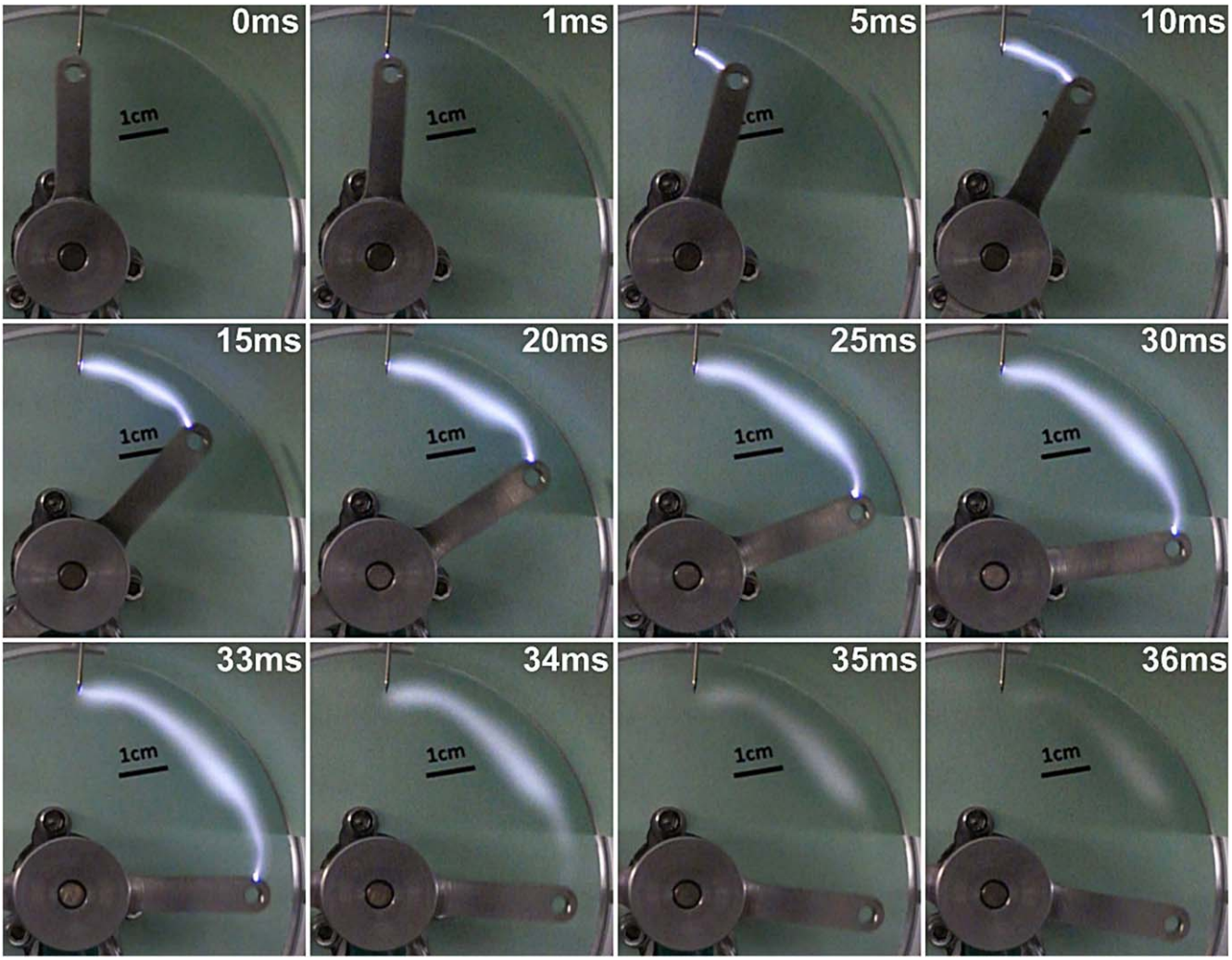

Figure 5. Time-resolved imaging of the discharge at 15 Hz and 9 kV using pulse modulation.

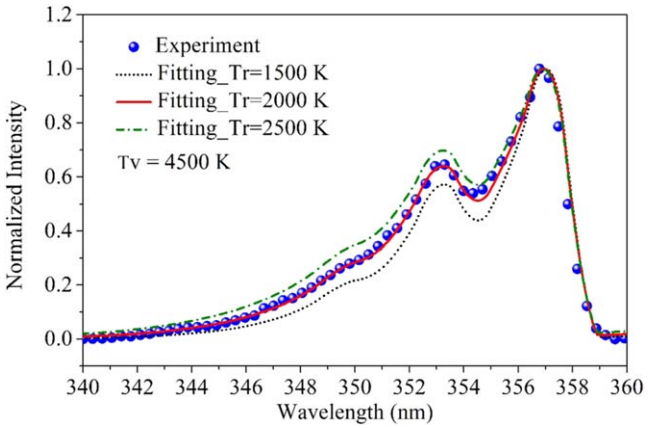

Figure 6. Experimental and fitting spectra of N_2. The applied voltage is 9 kV with pulse mode and the frequency is 15 H.

spark transition discharge; initially, the discharge is a streamer, which then transforms to a short spark pulse due to the discharging of the stray capacitance of the system. After breakdown, the PA discharge mode transforms into a structure similar to a glow discharge due to the ballast resistor-induced current limitation.

Figure 4 shows the discharge voltage and current waveforms of PA using a DC power supply. On a time scale of ms (figure 4(a)), we can see the applied voltage is fixed at 9 kV. The discharge voltage quickly drops to ∼0 from 9 kV as the discharge breaks down.

As shown in figure 4(c), the discharge current appears with a ∼20 ns pulse and a peak of 8 A during the breakdown. Then as seen in figure 4(a) V_{dis} shows some fluctuation in the ms timescale: it first increases to ∼1.3 kV, then decreases to 0.3 kV and finally quickly increases to 9 kV. This is due to the rotation of the cathode and the resulting extension of the plasma plume length. After ∼40 ms, the plasma is extinguished and current drops to zero. The total power consumption is ∼43 W as shown in figure 4(a). The breakdown region power consumption is ∼8 mW (figure 4(c)) which is about twice the value recorded using pulse modulation (see figure 3(c)). However, in both cases the breakdown-associated power dissipation can be neglected compared to the overall power consumption in PA. The DC powered case exhibits similar transient behavior with pulse modulation case in that the discharge appears similar to a transient spark during breakdown which then transitions to a glow-type

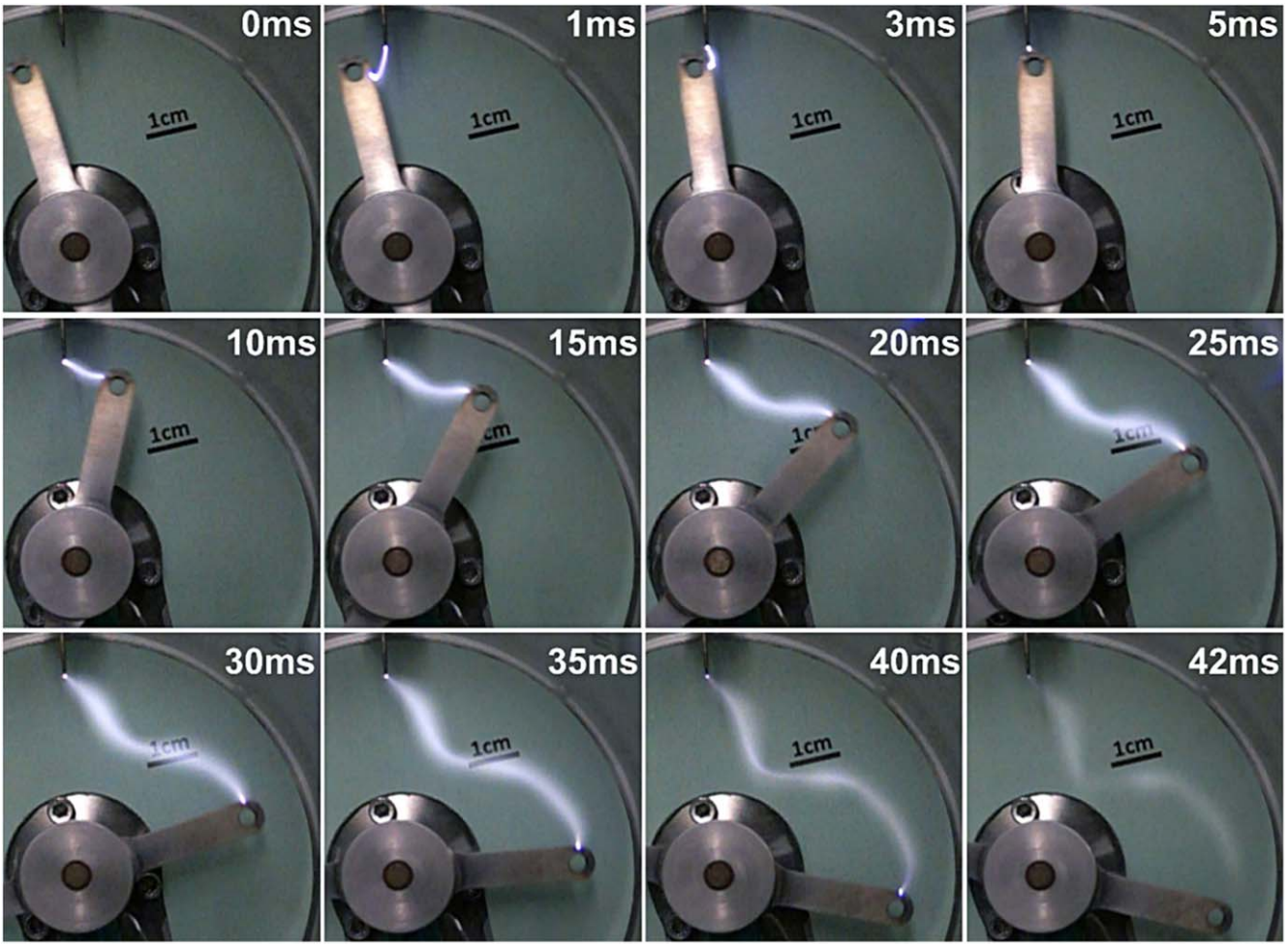

Figure 7. Time-resolved images of the PA discharge at 15 Hz and 9 kV using a DC power supply.

discharge. However, unlike the pulse modulation case, where the discharge voltage increases up to ∼3 kV until breakdown occurs, in the DC case, the breakdown occurs at the constant 9 kV resulting in higher power consumption in the discharge.

3.2. Time-resolved imaging of PA

Figure 5 shows time-resolved images of the PA discharge under the pulse modulation conditions associated with figure 3. A high-speed camera (Sony Cyber-shot, DSC-RX100 IV) is used to capture the images synchronized with the discharge current (see figure 3(a)). The frame rate is set at 1000 per second with a corresponding image exposure time of 1 ms. The plasma ignites at the narrowest gap (∼0.5 mm) between cathode and anode. The plasma plume is subsequently stretched by the rotating cathode. The PA discharge is visually stable and the brightest part of the visible plume is arc-shaped. A cathode spot can be seen near the tip of the rotating cathode during the pulse (0–33 ms). Interestingly, even after the applied voltage is zero (∼34 ms), the plasma plume is still visible. It suggests there are relatively long-lived species produced during the PA discharge. From the visual images (figure 5: 34–36 ms), the apparent lifetime is ∼3 ms.

Emission spectra from the N_2 second positive system was simulated and fitted to the measured OES data (via SpecAir software) [41] to estimate rotational and vibrational temperatures of nitrogen as shown in figure 6. The OES was measured near the stationary anode (1 cm close to the tip of anode). The applied voltage is 9 kV with pulse mode and the frequency is 15 H. The rotational and vibrational temperatures are estimated to be ∼2000 ± 500 K and ∼4500 ± 500 K during our experiment, respectively. The melting point of the steel is 1800 K, however, investigation of the cathode surface with microscope after several hours of operation revealed no indication of melting. Also, Wang *et al* [42], reported an estimated temperature of about 1500 K using a GA under similar experimental conditions to ours. We conclude, therefore, the gas temperature in our experiment is about 1500 K, however, we acknowledge this is only an estimate.

Figure 7 illustrates time-resolved images of the PA discharge using a DC power supply; this corresponds to the discharge current and voltage waveforms shown in figure 4(a). After the very short breakdown period, the plasma length fluctuates during the first few milliseconds (similar to V_{dis}). At ∼1 ms, the plasma presents a '*V*' shape with a length of ∼10 mm. Then it shortens to the gap minimum spacing as the cathode moves to the anode. As in the pulse modulation case, after ∼5 ms, the plasma plume is stretched by the rotating cathode. Notably, in the DC powered case, the

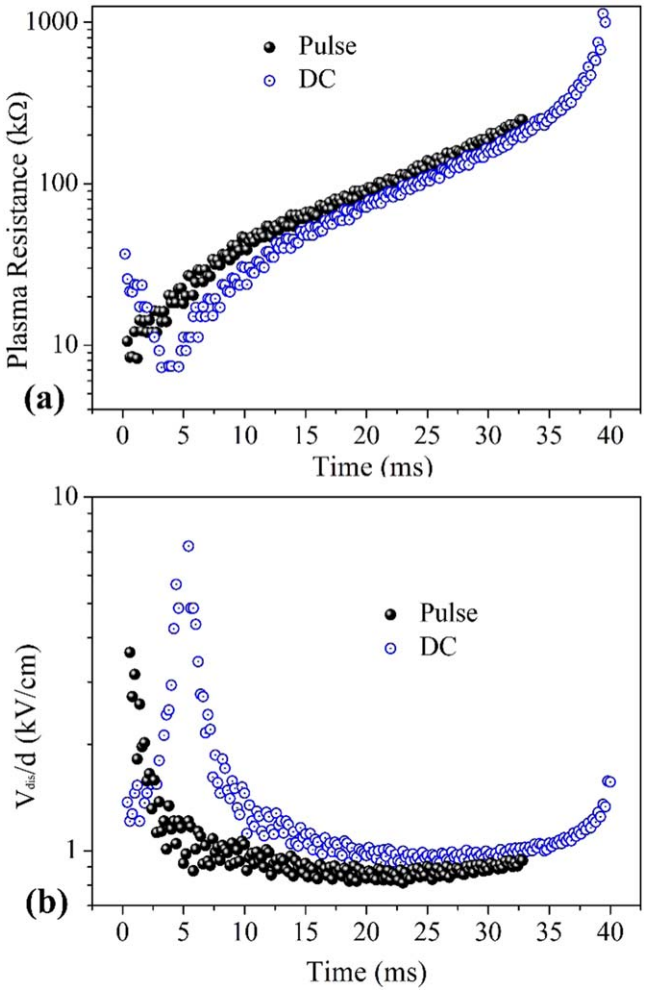

Figure 8. (a) Plasma resistance (V_{dis}/I_{dis}) and (b) average electric field V_{dis}/d versus discharge time using pulse modulation (black symbols) and DC power supply (blue symbols).

discharge lasts for a longer period of time, before the discharge gap becomes too large for the power supply to maintain the plasma. The plasma plume reaches a maximum of ~66 mm using our DC power supply.

3.3. Plasma resistance and average electric field V_{dis}/d

In order to further investigate the characteristics of the PA discharge, the plasma resistance and the spatially-averaged electric field (V_{dis}/d) are calculated based on the data shown in figure 8. PA instantaneous resistance is defined as V_{dis}/I_{dis}. In part, we compute these quantities because they may help in future attempts to understand the physico-chemical properties of the PA discharge. Note that over the short time (few-several ns) following breakdown, the resistance of the discharge is significantly lower. Janda *et al* [40] addressed this issue. In our paper we focused on the ms time scale, extending from breakdown to extinguishment.

In the pulse modulation case, the plasma resistance increases rapidly from ~8 to ~250 kΩ from breakdown to plasma extinction. For the DC power supply case, the plasma resistance first decreases to ~8 kΩ, after initially reaching ~40 kΩ, it then increases to almost 1000 kΩ as the plasma is extinguished. In the DC case, after 5 ms (corresponding to the point of the narrowest gap), the resistance profile matches that seen for pulse modulation.

The spatially-averaged electric field is defined by V_{dis}/d, where V_{dis} is the instantaneous gap discharge voltage and d is the instantaneous visible length of the PA plasma. From the time-resolved images shown in figures 5 and 7, d is nearly equal to the arc length from the tip of the anode to the tip of the cathode. We estimate the arc length assuming the arc is circular using the following expression:

$$d \approx t^{*}f^{*}L. \tag{2}$$

In (2), t is time elapsed after breakdown (s), f is the discharge frequency (in Hz, determined by the motor angular velocity) and L is the length of the half-circle traced by the propeller-like blade cathode. The latter value is calculated to be $\pi^{*}3.5 = 11$(cm). We note, as seen in figure 7, the shape of discharge can deviate from circular. Even in this case however, we find the plasma length estimated from images are within 5% of values estimated using expression (2).

Figure 8(b) plots average electric field V_{dis}/d versus discharge time using pulse modulation and the DC power supply. In the pulse modulation case, the average electric field starts at a value of ~4 kV cm^{-1} at breakdown, then drops within the first few ms. After about 5 ms, it maintains a relatively stable value of ~0.8 kV cm^{-1} up to ~33 ms with a slight rise at the end. It should be noted that plasma length and the electrical characteristics of PA change significantly during this time. In the DC power supply case, V_{dis}/d first increases to a peak of ~7.5 kV cm^{-1} at ~5 ms after ignition from ~1.2 kV cm^{-1}. After this peak value, corresponding to the minimum gap position, it qualitatively follows the trend seen in the pulse modulation case, with a value of ~0.9 kV cm^{-1} from 15 to 35 ms. In the final region before the discharge is extinguished (~35–40 ms), V_{dis}/d increases again to ~1.8 kV cm^{-1}. Both in plots of plasma resistance and average electric field, a 'kink' is apparent for the DC power supply case, associated with the early breakdown and voltage oscillation.

3.4. Effects of PA discharge frequency and multiple electrodes

Two possible modifications to the PA configuration are to change the rotation frequency of the motor and to add multiple electrodes. We first investigate the effect of rotation frequency. In the PA design, the discharge frequency is controlled by the rotation frequency of the electrodes. Figure 9(a) plots plasma power consumption as a function of discharge frequency (10–180 Hz). Power consumption versus frequency over this range shows no qualitative differences between the two power supply configurations—both initially are flat then decline monotonically with frequency over this range. The visual images shown in figure 9(b) shows the pulse modulation discharge structure (similar for DC power) does not change qualitatively with increasing frequency, however, the discharge appears to get dimmer, consistent with decrease in power. For both cases, we observe a higher power

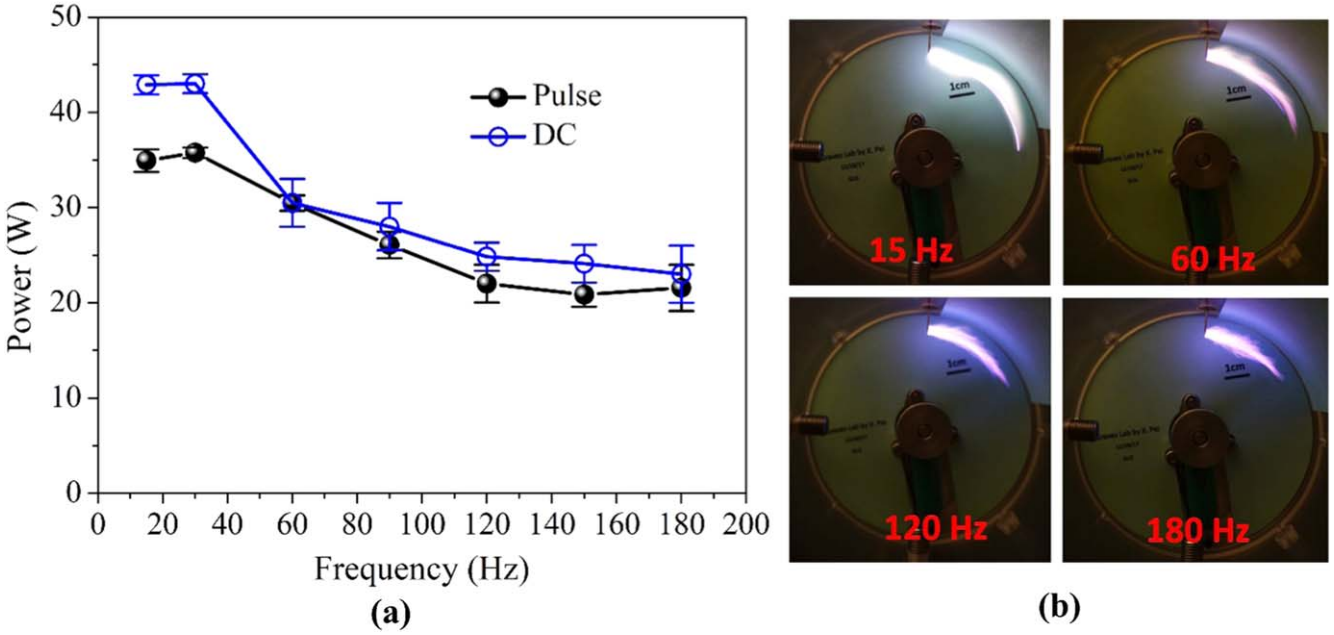

Figure 9. (a) Plasma power consumption and (b) corresponding discharge images (exposure time 1/20 s) under pulse modulation conditions, at different discharge frequencies and applied voltage 9 kV.

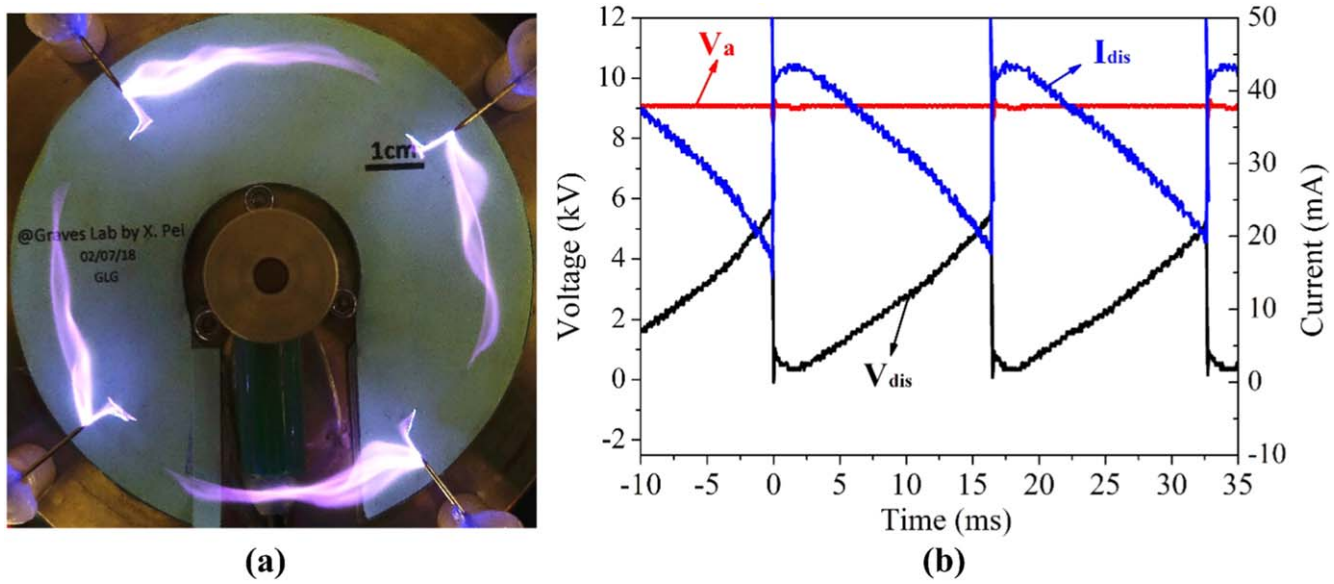

Figure 10. (a) Discharge image (exposure time 1/20 s) of PA using multiple electrodes at discharge frequency of 60 Hz; (b) discharge voltage and current using the DC power supply and multiple electrodes.

consumption at lower frequency. The mechanisms responsible for this behavior are not evident from our investigation. However, a potential explanation might involve the dynamics of processes essential for sustaining the discharge. The processes may be affected by the motion of the cathode blade, occurring at timescales of a few ms.

With the intention of improving the gas processing efficiency of the PA discharge, multiple electrodes are added to produce larger volume plasma. Figure 10(a) shows images of a case with four pin anodes with 2 two propeller-like cathode blades. Additional electrodes could be added, if desired. Figure 10(b) shows the PA discharge voltage and current waveforms when multiple electrodes are used. In this case, the total discharge power consumption reaches ∼132 W. This is actually only about three times the power consumed using a single electrode. As seen in figure 10(b) with a four-electrode configuration, a new discharge is ignited before the previous one can extinguish naturally. Based on this we conclude that in the PA configuration, using four electrodes discharge is being generated over most of the available volume, indicating no clear advantage in further increasing the number of electrodes at the examined rotation speeds.

4. Conclusions

A new non-equilibrium plasma source—the 'PA'—has been designed to produce a controllable, stable and relatively large volume plasma for high throughput gas processing applications. It consists of a rotating cathode, driven by a motor, with one or more fixed anodes. Similar to the widely-used GA, PA ignites when the local gap is near its narrowest position, and then stretches due to the rotating cathode, rather than by using forced or natural convection. With an applied voltage of 9 kV and peak current of ~45 mA, the length of the plasma column increases from 0.5 mm up to 66 mm using. PA exhibits two different discharge modes, similar to the transient spark during breakdown and to a glow discharge in the rest of discharge time. The plasma resistance changes from 8 to 1000 kΩ under our experimental conditions. The spatially-averaged electric field decreases from ~4 to ~1 kV cm^{-1} after breakdown, then tends to a stable value of 0.8 kV cm^{-1}. The power consumption of PA decreases with increasing electrode rotation frequency. We demonstrate the use of multiple electrodes to show that the PA can be easily expanded to larger volumes by establishing a discharge for larger fractions of the rotating cathode trajectory.

The device can be operated using pulse modulation or a DC power supply. The various aspects of the PA discharge is controlled more effectively using pulse modulation, including plasma plume length and the point of gas breakdown. However, pulse modulation requires a more complex device configuration including various sensing equipment, and time-triggered signals. The use of DC power is a simpler option, but the plasma ignition and extinguishment are not completely controlled and occurs naturally. Depending on the requirements of the specific applications, both operation modes may find a use.

In this paper, relatively simple examples using the concept of rotating electrodes have been presented. It is not difficult to imagine more complex and specialized versions of the design, including the use of multiple cathodes and anodes; modified diameter and shape of the rotating blade cathode; various changes in discharge power supply; coupling with gas flow control devices, etc. Due to its compact design, controllability and stability, the PA device configuration appears promising for many applications including nitrogen fixation, fuel conversion, carbon dioxide conversion, waste treatment, and hydrogen sulfide treatment, among others.

Acknowledgments

The authors gratefully acknowledge many useful discussions with Rune Ingels of N2Applied (Oslo Norway). This work was partially supported by the Department of Energy OFES grant #DE-SC0001939 and National Science Foundation Grant #1606062.

ORCID iDs

Xuekai Pei https://orcid.org/0000-0003-0423-2397
Dogan Gidon https://orcid.org/0000-0001-5832-4698

References

[1] Bruggeman P J, Iza F and Brandenburg R 2017 Foundations of atmospheric pressure non-equilibrium plasmas *Plasma Sources Sci. Technol.* **26** 123002
[2] Lu X, Laroussi M and Puech V 2012 On atmospheric-pressure non-equilibrium plasma jets and plasma bullets *Plasma Sources Sci. Technol.* **21** 034005
[3] Laroussi M and Fridman A 2008 Plasma medicine *Plasma Processes. Polym.* **5** 501–2
[4] von Woedtke T, Reuter S, Masur K and Weltmann K D 2013 Plasmas for medicine *Phys. Rep.-Rev. Sect. Phys. Lett.* **530** 291–320
[5] Pavlovich M J, Clark D S and Graves D B 2014 Quantification of air plasma chemistry for surface disinfection *Plasma Sources Sci. Technol.* **23** 065036
[6] Bruggeman P and Leys C 2009 Non-thermal plasmas in and in contact with liquids *J. Phys. D: Appl. Phys.* **42** 053001
[7] Choi Y H, Kim J H, Paek K H, Ju W T and Hwang Y S 2005 Characteristics of atmospheric pressure N-2 cold plasma torch using 60 Hz AC power and its application to polymer surface modification *Surf. Coat. Technol.* **193** 319–24
[8] Ding Y, He D Y and Shirai H 2009 Deposition of low dielectric constant SiOC films by using an atmospheric pressure microplasma jet *J. Phys. D: Appl. Phys.* **42** 125503
[9] Cherkasov N, Ibhadon A O and Fitzpatrick P 2015 A review of the existing and alternative methods for greener nitrogen fixation *Chem. Eng. Process.* **90** 24–33
[10] Patil B S, Wang Q, Hessel V and Lang J 2015 Plasma N-2-fixation: 1900–2014 *Catal. Today* **256** 49–66
[11] Ito M, Oh J S, Ohta T, Shiratani M and Hori M 2018 Current status and future prospects of agricultural applications using atmospheric-pressure plasma technologies *Plasma Process. Polym.* **15** e1700073
[12] Pei X, Lu X, Liu J, Liu D, Yang Y, Ostrikov K, Chu P K and Pan Y 2012 Inactivation of a 25.5 μm Enterococcus faecalis biofilm by a room-temperature, battery-operated, handheld air plasma jet *J. Phys. D: Appl. Phys.* **45** 165205
[13] Fanelli F and Fracassi F 2017 Atmospheric pressure non-equilibrium plasma jet technology: general features, specificities and applications in surface processing of materials *Surf. Coat. Technol.* **322** 174–201
[14] Czernichowski A 1994 Gliding arc—applications to engineering and environment control *Pure Appl. Chem.* **66** 1301–10
[15] Fridman A, Nester S, Kennedy L A, Saveliev A and Mutaf-Yardimci O 1999 Gliding arc gas discharge *Prog. Energy Combust. Sci.* **25** 211–31
[16] Czernichowski A, Nassar H, Ranaivosoloarimanana A, Fridman A A, Simek M, Musiol K, Pawelec E and Dittrichova L 1996 Spectral and electrical diagnostics of gliding arc *Acta Phys. Pol.* A **89** 595–603
[17] Balcon N, Benard N, Braud P, Mizuno A, Touchard G and Moreau E 2008 Prospects of airflow control by a gliding arc in a static magnetic field *J. Phys. D: Appl. Phys.* **41** 205204
[18] Gangoli S P, Gutsol A F and Fridman A A 2010 A non-equilibrium plasma source: magnetically stabilized gliding arc discharge: II. Electrical characterization *Plasma Sources Sci. Technol.* **19** 065004
[19] Gangoli S P, Gutsol A F and Fridman A A 2010 A non-equilibrium plasma source: magnetically stabilized gliding

arc discharge: I. Design and diagnostics *Plasma Sources Sci. Technol.* **19** 065003
[20] Lee H and Sekiguchi H 2011 Plasma-catalytic hybrid system using spouted bed with a gliding arc discharge: CH_4 reforming as a model reaction *J. Phys. D: Appl. Phys.* **44** 274008
[21] Nunnally T, Gutsol K, Rabinovich A, Fridman A, Gutsol A and Kemoun A 2011 Dissociation of CO_2 in a low current gliding arc plasmatron *J. Phys. D: Appl. Phys.* **44** 274009
[22] Kusano Y, Sorensen B F, Andersen T L, Toftegaard H L, Leipold F, Salewski M, Sun Z W, Zhu J J, Li Z S and Alden M 2013 Water-cooled non-thermal gliding arc for adhesion improvement of glass-fibre-reinforced polyester *J. Phys. D: Appl. Phys.* **46** 135203
[23] Zhao T L, Xu Y, Song Y H, Li X S, Liu J L, Liu J B and Zhu A M 2013 Determination of vibrational and rotational temperatures in a gliding arc discharge by using overlapped molecular emission spectra *J. Phys. D: Appl. Phys.* **46** 345201
[24] Korolev Y D, Frants O B, Landl N V, Bolotov A V and Nekhoroshev V O 2014 Features of a near-cathode region in a gliding arc discharge in air flow *Plasma Sources Sci. Technol.* **23** 054016
[25] Whitehead J C and Prantsidou M 2016 Investigation of hydrocarbon oil transformation by gliding arc discharge: comparison of batch and recirculated configurations *J. Phys. D: Appl. Phys.* **49** 154001
[26] Bosi F J and Dobrynin D 2017 Gliding arc plasma assisted N_2O dissociation for monopropellant propulsion *J. Phys. D: Appl. Phys.* **50** 025202
[27] Gao J L, Zhu J J, Ehn A, Alden M and Li Z S 2017 *In-situ* non-intrusive diagnostics of toluene removal by a gliding arc discharge using planar laser-induced fluorescence *Plasma Chem. Plasma Process.* **37** 433–50
[28] Zhu J J *et al* 2015 Measurements of 3D slip velocities and plasma column lengths of a gliding arc discharge *Appl. Phys. Lett.* **106** 044101
[29] Richard F, Cormier J M, Pellerin S and Chapelle J 1996 Physical study of a gliding arc discharge *J. Appl. Phys.* **79** 2245–50
[30] Pellerin S, Richard F, Chapelle J, Cormier J M and Musiol K 2000 Heat string model of bi-dimensional dc Glidarc *J. Phys. D: Appl. Phys.* **33** 2407–19
[31] Sperka J, Soucek P, Van Loon J J W A, Dowson A, Schwarz C, Krause J, Kroesen G and Kudrle V 2013 Hypergravity effects on glide arc plasma *Eur. Phys. J.* D **67** 261
[32] Fridman A, Gutsol A, Gangoli S, Ju Y G and Ombrellol T 2008 Characteristics of gliding arc and its application in combustion enhancement *J. Propulsion Power* **24** 1216–28
[33] Kalra C S, Cho Y I, Gutsol A, Fridman A and Rufael T S 2005 Gliding arc in tornado using a reverse vortex flow *Rev. Sci. Instrum.* **76** 025110
[34] Kalra C S, Gutsol A F and Fridman A A 2005 Gliding arc discharges as a source of intermediate plasma for methane partial oxidation *IEEE Trans. Plasma Sci.* **33** 32–41
[35] Gallagher M J, Geiger R, Polevich A, Rabinovich A, Gutsol A and Fridman A 2010 On-board plasma-assisted conversion of heavy hydrocarbons into synthesis gas *Fuel* **89** 1187–92
[36] Ramakers M, Trenchev G, Heijkers S, Wang W Z and Bogaerts A 2017 Gliding arc plasmatron: providing an alternative method for carbon dioxide conversion *ChemSusChem* **10** 2642–52
[37] Wu A J, Yan J H, Zhang H, Zhang M, Du C M and Li X D 2014 Study of the dry methane reforming process using a rotating gliding arc reactor *Int. J. Hydrog. Energy* **39** 17656–70
[38] Zhang H, Du C M, Wu A J, Bo Z, Yan J H and Li X D 2014 Rotating gliding arc assisted methane decomposition in nitrogen for hydrogen production *Int. J. Hydrog. Energy* **39** 12620–35
[39] Czernichowski A 1999 Plasmas for destruction of H_2S and mercaptans *Oil Gas Sci. Technol.* **54** 337–55
[40] Janda M, Martisovits V and Machala Z 2011 Transient spark: a dc-driven repetitively pulsed discharge and its control by electric circuit parameters *Plasma Sources Sci. Technol.* **20** 035015
[41] Machala Z, Janda M, Hensel K, Jedlovsky I, Lestinska L, Foltin V, Martisovits V and Morvova M 2007 Emission spectroscopy of atmospheric pressure plasmas for bio-medical and environmental applications *J. Mol. Spectrosc.* **243** 194–201
[42] Wang W, Patil B, Heijkers S, Hessel V and Bogaerts A 2017 Nitrogen fixation by gliding arc plasma: better insight by chemical kinetics modelling *ChemSusChem* **10** 2145–57